vehicles

MDPI

Article

Modeling Nighttime Traffic Risk Through Static Infrastructure Typology and Dynamic Environmental Interactions

Pengpeng Xie [1], Gang Fu [2], Lei Xu [1,*], Yong Peng [3], Xingchang Wang [4], Chaojie Fan [3] and Jiandong Hu [5]

[1] School of Mechanical and Automotive Engineering, Guangxi University of Science and Technology, Liuzhou 545006, China; paulxie@gxust.edu.cn
[2] Traffic Police Detachment of Liuzhou Public Security Bureau, Liuzhou 545025, China; jjzdsgk@126.com
[3] School of Traffic & Transportation Engineering, Central South University, Changsha 410075, China
[4] Beijing Chenrong Testing Technology Co., Ltd., Beijing 100005, China
[5] Guangdong Zhongzhi Institute of Forensic Trace Identification, Foshan 528000, China
* Correspondence: 2020018@gxust.edu.cn

Abstract

To address the high frequency of nighttime urban road traffic crashes and the lack of models that adequately quantify the traffic risks, this study develops a dual-layer model that couples static baseline risk with dynamic environmental corrections. Using the analytic hierarchy process and expert judgment, we determine baseline weights for nine road types: intersections (0.198), access points (0.162), curves/narrow roads (0.146), bridges (0.113), internal roads (0.095), tunnels (0.083), road segments (0.071), crosswalks (0.067), and ramps (0.066). Illumination, weather, and time are incorporated as dynamic environmental factors to enable nonlinear weight adjustment. Furthermore, total traffic risk is divided into five levels: low [0, 0.10), mild [0.10, 0.25), moderate [0.25, 0.45), high [0.45, 0.80), and critical [0.80, 1.00]. Quantitative risk analysis reveals that under extreme conditions of no illumination and heavy rain, the risk at intersections reaches 0.388, which is 1.53 times the risk under bright and clear conditions (0.254). Validation using 40,852 nighttime crash records shows that visibility (OR = 1.65) and illumination (OR = 0.56) are the most significant factors affecting crash severity, while weather (OR = 0.89) and time (OR = 0.96) show moderate effects. This study provides a basis for prioritizing lighting improvements and issuing proactive warnings for adverse weather and late-night periods.

Keywords: nighttime traffic crash; traffic risk; road attributes; road illuminations; risk quantification

Check for updates

Academic Editor: Anna Granà

Received: 23 July 2026
Revised: 2 October 2026
Accepted: 10 October 2026
Published: 20 October 2026

Copyright: © 2026 by the authors. Licensee MDPI, Basel, Switzerland. This article is an open access article distributed under the terms and conditions of the Creative Commons Attribution (CC BY) license.

1. Introduction

Nighttime road traffic safety is a common challenge faced by countries around the world. Statistics show that approximately 40–50% of traffic crashes occur at night, despite nighttime driving accounting for less than 20% of the total travel distance [1]. This poses a severely disproportionate threat that underscores the unique hazards of the nighttime driving environment.

The mechanisms underlying nighttime crashes differ fundamentally from those during the daytime. Daytime crashes are often associated with traffic volume, driver-related factors, and driving behavior, whereas nighttime crashes are more likely to result from the interaction between the traffic environment and drivers' physiological, psychological, and behavioral states [2,3]. Under low illumination, drivers experience degraded visual function, prolonged reaction times, and distorted speed perception. Compounded by the

effects of circadian rhythms, fatigue and reduced alertness are particularly pronounced at night [4]. This coupling mechanism involving environmental, physiological, and behavioral factors makes the causations of nighttime crashes more complex.

The intrinsic mechanisms by which different road types contribute to crashes also vary substantially. Intersections contain dense vehicle–vehicle and vehicle–pedestrian conflict points and impose high decision-making demands [5]. Bridges may be affected by crosswinds, alignment changes, and visibility constraints [6,7]. Tunnel portals can produce abrupt luminance transitions and visual-adaptation burdens associated with black-hole/white-hole effects [8,9]. Ramp and access-point merging areas are characterized by speed differences, gap-acceptance decisions, and merging conflicts [10,11]. These structural characteristics constitute relatively stable intrinsic attributes of nighttime traffic risk and therefore need to be explicitly represented in the assessment process. Thus, it is of great importance to accurately quantify nighttime traffic risk and reveal coupling mechanisms for improving road traffic safety, as well as developing active safety warning systems, and advancing autonomous driving technology [12]. Quantitative assessment provides a scientific basis for traffic management agencies to optimize lighting facilities and formulate differentiated control strategies. Therefore, establishing a nighttime traffic risk quantification method that accounts for both static road attributes and dynamic environmental disturbances holds substantial theoretical value and practical significance.

Nighttime road traffic risk has been examined from multiple dimensions, including exposure, environmental conditions, road structure, driver characteristics, crash-severity modeling, and safety interventions [5,13,14]. Nighttime crash risk exhibits pronounced spatiotemporal and demographic characteristics. The first factor that poses threat to traffic is nighttime environments. Study indicates that nighttime fatality risk is approximately 1.3 times higher than during daytime, with pedestrians and motorcyclists accounting for most deaths, and 67% of crashes concentrated between 18:00 and 22:00 [13]. Studies have verified that low illumination prolongs reaction time by impairing rod cell function, thereby increasing braking distance [15]. Road markings and traffic signs can improve nighttime driving behavior and reduce stress levels, particularly among young drivers [16]. On the other hand, environmental conditions further modulate risk. Both low and high temperatures, reduced visibility, and weekend nighttime periods are associated with significantly elevated crash risk [17].

The second factor is the driver's psychological and physiological states. Drivers tend to severely overestimate pedestrian visibility at night and fail to compensate through appropriate use of high beams or speed reduction [18]. Driver characteristics also contribute substantially to nighttime crashes. Myopic drivers exhibit poorer nighttime driving ability than non-myopic individuals [19]. Experienced drivers report visibility-related hazards more frequently than novices, suggesting that hazard perception improves with accumulated driving experience [20]. Temporal instability in crash severity factors has been observed between older and middle-aged drivers, with early morning hours posing particular risk [21]. Virtually, the risk factors mentioned above always interact to induce crashes. In highway work zones, factors such as elderly drivers, males, lane closures, and side collisions play a more prominent role at night [22]. In entrance and exit zones, a luminance threshold effect exists—once illumination reaches a certain level, safety outcomes stabilize [23].

Modeling approaches for nighttime crashes have diversified. A multi-stage consensus model incorporating circadian rhythms captures biological influences on driver performance [24], while GIS with data mining has classified crash patterns, revealing the predominance of motorcycle crashes and the roles of speeding and wrong-way driving [25], and regression comparisons identify morning peak, evening peak, and nighttime as the strongest correlates of crash occurrence [26]. Algorithms such as ThunderGBM on digital twin platforms show strong detection capability, and hybrid TimeSformer–LSTM–attention architectures enable real-time severity identification [27]. Machine learning models have also predicted crash severity using multidimensional data [28]. Intervention strategies span exposure reduction, crash prevention, injury mitigation, and pre-hospital care [29]. Traffic sign detection varies between day and night, with reflective material properties playing a critical role [30]. Fatigue detection systems based on image enhancement and facial recognition support active nighttime safety [31,32], and analyses of speeding and drunk driving identify male drivers, private vehicles, unlit nighttime conditions, and poor visibility as significant risk factors, providing a basis for targeted enforcement [33].

Although existing research has yielded substantial achievements in nighttime traffic-safety analysis, systematic quantification of the inherent risk differences among road types remains limited. In addition, the nonlinear coupling between relatively stable infrastructure-related risk and dynamic factors such as illumination, weather, and time has received less attention than crash occurrence or severity prediction [5,14,28]. Large-scale empirical validation using real-world nighttime crash records is also important for assessing whether the risk mechanisms represented by a model are consistent with observed crash-severity patterns. To address these research gaps, this study takes Liuzhou City as a case study and develops a two-tier nighttime traffic risk quantification model consisting of a static baseline risk component and a dynamic environmental adjustment component. The main contributions are as follows:

(1) Drawing on crash frequency, crash severity, risk avoidability, and environmental sensitivity, the analytic hierarchy process (AHP) combined with expert panel methods is employed to determine the comprehensive weights of nine road types: intersections, entrances and exits, bridges, internal roads, tunnels, road segments, ramps, crosswalks, and curved/narrow roads.
(2) Three dynamic environmental factors including lighting, weather, and time are incorporated, and a variable weight synthesis method is adopted to achieve nonlinear dynamic adjustment of risk weights. Thereby, a fusion model is established in which the baseline risk is multiplied by a dynamic correction coefficient.
(3) Using 40,852 nighttime traffic crash records from 2018 to 2024, ordinal logit regression method is conducted to analyze the influence of various risk factors on crash severity, thereby validating the effectiveness of the proposed model.

2. Materials and Methods

Figure 1 illustrates the overall research framework of this study. The workflow consists of four main stages. First, the crash data are collected and preprocessed. Second, the static baseline risk is determined using AHP combined with expert panel decision-making. Third, three dynamic environmental factors are incorporated through variable weight synthesis to achieve nonlinear risk adjustment. Fourth, the total risk is quantified, validated using ordinal logit regression, and visualized through risk heatmaps and temporal evolution analysis. Finally, policy implications are derived based on empirical findings.

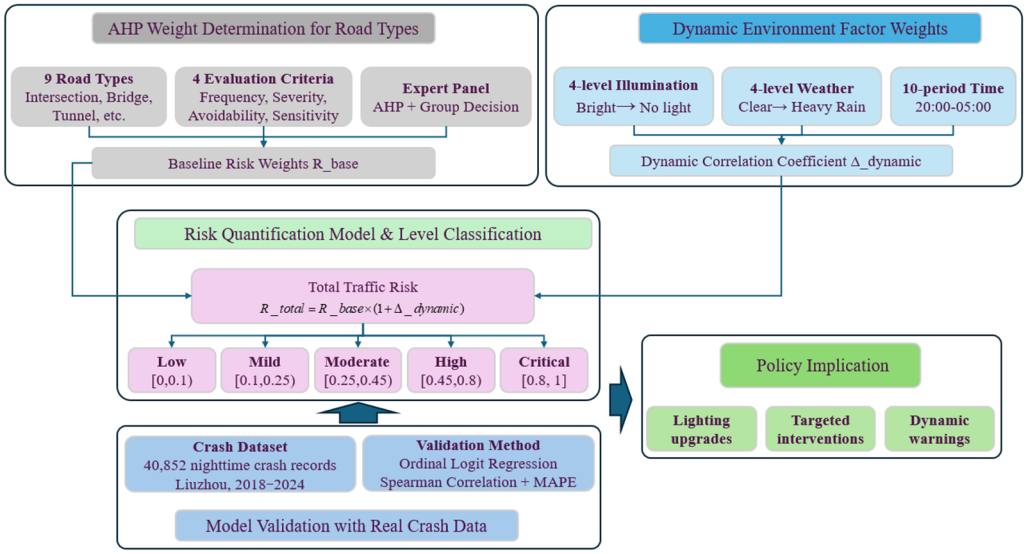


Figure 1. Flowchart of the research methodology.

2.1. Decision Framework for Weight Assignment

Weight assignment directly determines the accuracy of risk magnitude and prediction. This study establishes a four-dimensional evaluation framework covering crash frequency, crash severity, risk avoidability, and environmental sensitivity.

Dimension I is crash frequency. In the AHP evaluation process, experts were asked to assess the relative crash frequency of different road types based on volume-adjusted crash rates (number of crashes per 10,000 vehicles), rather than absolute crash counts. Traffic volume data (average annual daily traffic) for each road type were provided to the panel to ensure that their assessments reflected exposure-adjusted risk. This approach accounts for the fact that road segments typically carry much higher traffic volumes than other road types, and absolute crash counts alone would be misleading for cross-type comparisons.

Dimension II is crash severity, which uses equivalent property damage costs or casualty weight coefficients. It is noteworthy that crash severity is classified into three levels from fatal crashes, injury crashes, and property-damage-only crashes. Dimension III is risk avoidability. This dimension assesses the ease with which risk can be reduced through engineering improvements or intelligent warning systems. Measures such as warning signs, flashing yellow lights, ground-embedded lighting, and speed bumps can enhance warning effectiveness and improve driver responsiveness [34]. Dimension IV is environmental sensitivity. This dimension evaluates the extent to which risk deteriorates under adverse weather conditions such as rain, snow, or fog. High degree of deterioration corresponds with an upward adjustment of the comprehensive weight.

Meanwhile, according to the expertise of professionals in the field of traffic crash prevention, the risk weights for different road types are determined by combining group decision-making with AHP. Six experts who has years of crashes handling and managements were involved, and a review panel is established. In detail, two scholars are from universities who have engaged in road traffic safety research, two technical experts from enterprises specializing in crash management and causal analysis, and two officers from the traffic police department with extensive experience in traffic safety. Based on their practical experience in crash investigation, the panel members performed pairwise comparisons of the road types to provide relative importance judgments. Figure 2 presents the AHP hierarchical structure.

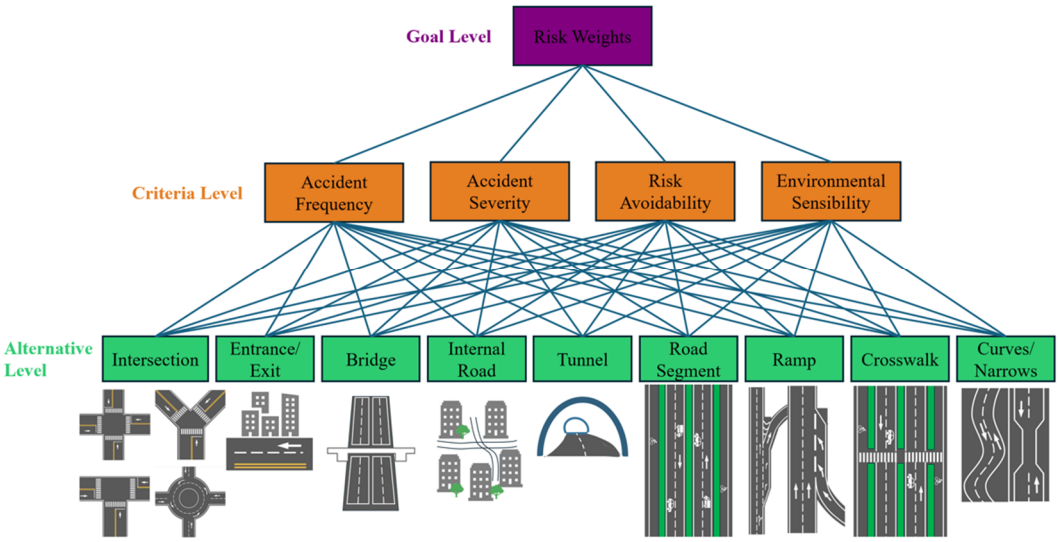


Figure 2. AHP hierarchical structure for weight determination.

Based on the group decision-making method, decision weights of 1, 2, and 3 were assigned to experts from universities, enterprises, and the traffic police department, respectively. Traffic police officers possess firsthand and comprehensive knowledge of local traffic characteristics, high-crash locations, and typical crash patterns derived from daily enforcement and crash investigation. Their direct operational experience ensures that the resulting risk coefficients are closely aligned with actual traffic conditions. Enterprise technical experts have practical experience in crash management and causation analysis, though their coverage of the entire road network may be less systematic than that of police officers. University scholars contribute theoretical rigor and methodological expertise but may lack direct operational experience with local nighttime traffic conditions. This weighting scheme was reviewed and collectively endorsed by all panel members prior to the pairwise comparison process, ensuring that the scheme reflects the consensus of the expert group rather than being imposed externally. It should be emphasized that the expert pairwise comparisons were based on the panel members' professional knowledge and field experience in nighttime crash investigation and road safety management. No crash records, exposure-normalized crash rates, or other quantitative summaries from the study dataset were disclosed to the experts during the AHP evaluation. The resulting baseline weights are therefore independent of the crash dataset used for model calibration and validation.

For each judgment matrix, the geometric mean method was employed to calculate the weight vectors for both the criterion layer and the alternative layer. First, the geometric mean of each row in the judgment matrix was computed using Equation (1), followed by normalization using Equation (2) to obtain the weight vector. Next, the maximum eigenvalue $\lambda_{\max}$, consistency index (CI), and consistency ratio (CR) were calculated using Equation (3) to perform consistency testing. A CR value of less than 0.1 indicates that the judgment matrix achieves satisfactory consistency. Finally, the comprehensive weight for each road type was determined using Equation (4).

$$M_i = \sqrt[n]{\prod_{j=1}^{n} a_{ij}}, i = 1, 2, \ldots, n \quad (1)$$

$$w_i = M_i \Big/ \sum_{j=1}^{n} M_j, i = 1, 2, \ldots, n \quad (2)$$

$$\lambda_{\max} = 1/n \cdot \sum_{i=1}^{n} (A \cdot w)_i / w_i, i = 1, 2, \ldots, n \quad (3)$$

$$R_{base_i} = \sum_{j=1}^{4} w_j \cdot w_{ij}, i = 1, 2, \ldots, n \quad (4)$$

where:

R_{base_i} is the comprehensive weight of the i-th road type;
w_j is the weight of the j-th criterion;
w_{ij} is the weight of the i-th road type with respect to the j-th criterion.

2.2. Dynamic Weight Adjustment Strategy

Nighttime lighting conditions, weather conditions, and time periods are selected as dynamic environmental factors, and the hierarchical variable weight method is adopted to achieve dynamic adjustment of risk weights. When a given risk factor deteriorates, its weight increases nonlinearly to reflect the factor's amplifying effect on the overall risk. Conversely, when multiple factors deteriorate simultaneously, the weight growth is moderately suppressed to prevent excessive inflation of the overall risk. In all cases, the sum of all factor weights remains equal to 1.

According to the Standard for Lighting Design of Urban Roads (CJJ45-91/2015) [35], as shown in Table 1, illuminations at night are divided into four levels.

Table 1. Standard for Lighting Design of Urban Roads.

Illumination Level	Illumination Ranges (lx)	Specifications
None	0–1	no artificial lighting, relying solely on vehicle headlights, moonlight, and other natural light sources
Low	1–10	branch roads or residential area roads
Normal	10–30	secondary arterial roads or primary arterial roads
Bright	≥30	main urban areas, commercial districts, and urban expressways

In addition, the weather conditions are classified into four levels ranging from heavy rain to clear. It is noteworthy that each level for both illumination and weather is assigned with a normalized value of within 1. Meanwhile, time is encoded from 0 to 9, which corresponds to the time from 20:00 PM to 05:00 AM. Table 2 shows the normalized values and baseline weights for dynamic risk factors. The baseline weights for the three dynamic factors were determined through a two-stage approach. In the first stage, the expert panel proposed initial weights based on their collective field experience in nighttime crash investigation. The panel reached a consensus that illumination is the most influential dynamic factor, as degraded lighting directly impairs visual perception and increases reaction times. Weather was ranked second, as it affects both visibility and road surface friction, while time was deemed least influential among the three, as its effect is primarily mediated through traffic volume variations. In the second stage, these initial weights were refined through model calibration. Specifically, we systematically varied each weight within a ±15% range and computed the corresponding risk scores for all road types under various environmental scenarios. The calibration objective was to maximize the Spearman correlation coefficient between the aggregated predicted risk scores and the observed crash

rates derived from the 40,852 crash records. The final weights (0.45, 0.29, 0.26) yielded the highest correlation ($\rho = 0.852$, $p < 0.01$) and were therefore selected. This two-stage approach ensures that the weights are not only grounded in practical expertise but also empirically validated against real-world crash data.

Table 2. Normalized values and baseline weights for dynamic risk factors.

Dynamic Risk Factor	Ordinal Variable xi	Normalized Value xi	Baseline Weight	Specification
Lighting	[None, Low, Normal, Bright]	[1, 0.8, 0.5, 0]	0.45	It depends on the Standard for Lighting Design of Urban Roads (CJJ45-91/2015)
Weather	[Heavy, Moderate, Light, Clear]	[1, 0.6, 0.3, 0.1]	0.29	Based on the meteorological severity classification
Time	[20:00 p.m.–06:00 a.m.]	exp-0.1582x	0.26	Derived from nighttime traffic volume decay pattern

Using the variable weight synthesis method, the dynamic weight $dynamic_w_i$ of the i-th risk factor is expressed as shown in Equation (5).

$$f_i(X_i) = dynamic_w_i^0 \cdot x_i^{\alpha-1} \Big/ \sum_{j=1}^{3} dynamic_w_j^0 \cdot x_j^{\alpha-1} \quad (5)$$

where:

$f_i(X_i)$ is the adjusted weight of the i-th risk factor;
x_i is the normalized risk value of the i-th risk factor;
$dynamic_w_i^0$ is the baseline weight of the i-th factor;
α is the variable weight coefficient, with $\alpha > 0$.

The variable-weight coefficient α governs the sensitivity of dynamic weight adjustment. When $\alpha = 1$, the model represents a normal weighting scheme without amplification. When $\alpha > 1$, an incentive-type variable weighting is applied, meaning that higher risk leads to a disproportionately larger weight. When $0 < \alpha < 1$, a penalty-type weighting is applied.

In this study, $\alpha = 1.5$ was selected through model calibration. Specifically, we tested α values from 0.5 to 3.0 at intervals of 0.1. For each α, we calculated the total risk scores for all road types under all environmental scenarios and computed the Spearman correlation coefficient between the predicted risk scores and the observed crash rates derived from the 40,852 crash records. The correlation coefficient reached its maximum ($\rho = 0.852$, $p < 0.01$) at $\alpha = 1.5$, which was therefore adopted.

2.3. Traffic Risk Modeling

As nighttime traffic risks are closely associated with road types and dynamic environments including road illuminations and weather, we employ a modeling approach that decomposes traffic risk into two hierarchical layers: static intrinsic attributes and dynamic time-varying disturbances. This is a methodology widely applied in engineering safety and other fields. The core idea of this framework is that the risk of any entity can be regarded as the combined result of its inherent risk and external environmental disturbances. Specifically, the baseline risk R_{base} represents the inherent risk attributes of a given road type, which is determined by relatively stable factors such as structural design. For instance, intersections naturally exhibit a higher baseline risk due to their dense conflict points. Such conflict points do not change with instantaneous environmental variations. $\Delta_{dynamic}$ is the dynamic risk correction coefficient as shown in Equation (6). It reflects the amplifying

or attenuating effects of time-varying factors such as environment, traffic, and time on risk, while the dynamic correction coefficient ($1 + \Delta_{\text{dynamic}}$) captures the amplifying or mitigating effects of spatiotemporal environmental factors on the baseline risk. Finally, the total traffic risk is calculated using a linear superposition method, as shown in Equation (7).

$$\Delta_{dynamic} = \sum_{i=1}^{3} f_i(X_i) \cdot x_i \tag{6}$$

$$R_{total} = R_{base} \times (1 + \Delta_{dynamic}) \tag{7}$$

To make full use of the quantified risk outcomes, traffic risk is divided into five levels, namely low risk, relatively low risk, moderate risk, high risk, and extremely high risk. The risk ranges corresponding to each risk level are shown in Figure 3.

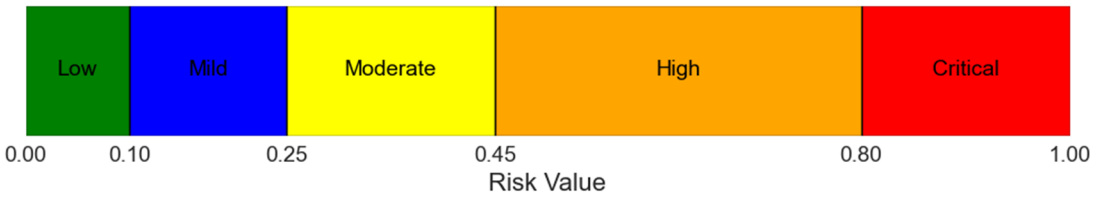


Figure 3. The criteria for dividing traffic risk levels.

In Figure 3, low risk level indicates that current nighttime driving conditions are favorable, and drivers can drive normally. The relatively low risk level suggests that drivers need to maintain a certain level of alertness and pay attention to traffic conditions. Moderate risk means the road has significant hazards, and the drivers should mind their speed and prepare to brake or decelerate. When the risk reaches the high or extremely high level, it signifies hazardous driving conditions, and it is strongly recommended that drivers exercise extreme caution or take evasive actions.

The risk level thresholds presented in Figure 3 were established through a collaborative expert consultation process. A panel of specialists was convened, comprising traffic police officers with extensive experience in nighttime crash investigation and road safety management, technical experts from traffic safety enterprises specializing in crash causation analysis and risk control interventions, and scholars from universities engaged in road traffic safety research. The panel reviewed the calculated risk values across representative scenarios and reached a consensus on the threshold intervals through an iterative consultation process. The final thresholds reflect the panel's collective professional judgment regarding drivers' perceived risk, vehicle controllability, and crash likelihood under various nighttime conditions.

It should be noted that these empirically derived thresholds, while practically grounded, are not directly drawn from existing literature, as no prior studies have established explicit risk-level boundaries for nighttime traffic risk quantification using a comparable dual-layer modeling framework.

2.4. Model Selection

The ordinal logit regression model was selected as the primary validation method for several considerations. As our goal is to quantify the marginal effects of individual risk factors on crash severity to inform targeted safety interventions, ordinal logit regression yields odds ratios that are directly interpretable. In contrast, machine learning algorithms such as random forest, gradient boosting, or neural networks, while often achieving higher predictive accuracy, operate as "black-box" models and do not readily provide transparent marginal effect estimates for each explanatory variable [36].

On the other hand, model parsimony and stability favor the ordinal logit approach. The proportional odds assumption is reasonably satisfied for our dataset, and the model converges efficiently with stable parameter estimates. Random parameters models, though capable of capturing unobserved heterogeneity, require computationally intensive estimation and may not yield reliable identification without more varied data structures [37].

In addition, it is important to clarify that ordinal logit regression serves as a validation tool rather than the core contribution of this study. Our primary methodological contribution is the dual-layer risk quantification framework. For validation purposes, a transparent and widely accepted statistical method that facilitates direct comparison with existing crash severity studies is preferred over a purely predictive algorithm. Nevertheless, we acknowledge that future research could employ machine learning or random parameters approaches to capture potential non-linear interactions and unobserved heterogeneity, which may further enrich the understanding of nighttime crash mechanisms.

2.5. Data Description

The crash data used in this study were obtained from the Liuzhou Public Security Bureau Traffic Police Detachment, covering a seven-year period from January 2018 to December 2024. A total of 40,852 nighttime crashes occurring between 20:00 and 06:00 were extracted from the comprehensive traffic crash database. The dataset includes detailed information on each crash, such as crash time, location (road type), crash severity, weather conditions, illumination conditions, visibility, and road pavement type.

Data cleaning procedures were applied prior to analysis. Records with missing values for key variables (crash severity, road type, or illumination) were excluded, resulting in a final sample of 40,852 valid observations. Table 3 presents the descriptive statistics for all variables included in the ordinal logit regression analysis.

Table 3. Descriptive statistics of the nighttime crash data (N = 40,852).

Variable	Category	Frequency	Percentage (%)
Crash Severity	Property-damage-only	34,256	83.9
	Injury	5633	13.8
	Fatal	963	2.3
Illumination	Bright	14,502	35.5
	Normal	11,594	28.4
	Low	9070	22.2
	None/Dark	5686	13.9
Weather	Clear	20,712	50.7
	Cloudy/Light Rain	10,098	24.7
	Moderate rain/Fog	6176	15.1
	Heavy Rain	3866	9.5
Visibility	>200 m	18,799	46.0
	100–200 m	10,416	25.5
	50–100 m	6542	16.0
	<50 m	5095	12.5

As shown in Table 3, the crash severity distribution is imbalanced, with property-damage-only crashes accounting for the majority (83.9%), followed by injury crashes (13.8%) and fatal crashes (2.3%). This imbalance is typical of real-world crash data and does not pose a problem for ordinal logit regression, which is specifically designed to handle ordered categorical outcomes with unequal category sizes.

3. Results

3.1. Baseline Risk Weights

Based on the scoring by experts from various fields and the group decision-making method for weight determination, the judgment matrices for the criterion layer and the alternative layer were calculated.

To ensure the reliability of the pairwise comparisons, several consistency parameters are calculated for each judgment matrix. The λ_{max} of each judgment matrix is first computed. The consistency index (*CI*) is then calculated using Equation (8).

$$CI = \frac{\lambda_{max} - n}{n - 1} \tag{8}$$

where n is the order of the judgment matrix. The consistency ratio (*CR*) is further derived by Equation (9):

$$CR = \frac{CI}{RI} \tag{9}$$

where *RI* is the random consistency index. The *RI* values for matrices of different orders are adopted from Saaty's standard table. A judgment matrix is considered to have satisfactory consistency when $CR < 0.1$. The consistency test results for each matrix, obtained using Equations (1)–(3), are shown in Table 4.

Table 4. Consistency of the criteria and alternative layer.

Judgment Matrices	*n*	λ_{max}	*CI*	*RI*	*CR*
Criteria Layer	4	4.117	0.039	0.89	0.044
Crash Frequency	9	9.312	0.039	1.46	0.027
Crash Severity	9	9.278	0.035	1.46	0.024
Risk Avoidability	9	9.195	0.024	1.46	0.016
Environmental Sensibility	9	9.145	0.018	1.46	0.012

As shown in Table 4, the *CR*s of each judgment matrix is less than 0.1, indicating that the judgment matrices established based on expert scoring have good consistency. The comprehensive weights of each road type were calculated according to Equation (4), and the results are presented in Table 5.

Table 5. Comprehensive weight matrix for all road types.

Road Type	Frequency (0.563)	Severity (0.265)	Risk Avoidability (0.123)	Environmental Sensitivity (0.049)	Comprehensive Weight
Intersection	0.212	0.195	0.165	0.152	0.198
Access Point	0.168	0.158	0.148	0.140	0.162
Bridge	0.110	0.112	0.118	0.118	0.113
Internal Road	0.092	0.094	0.102	0.110	0.095
Tunnel	0.081	0.078	0.092	0.098	0.083
Road Section	0.068	0.068	0.08	0.088	0.071
Ramp	0.062	0.060	0.082	0.102	0.066
Crosswalk	0.058	0.068	0.090	0.106	0.067
Curves/Narrows	0.149	0.167	0.115	0.086	0.146

As shown in Table 5, the comprehensive weights, in descending order, are as follows: intersection > entrance/exit > curves/narrows > bridge > internal road > tunnel > road section > ramp > crosswalk.

In nighttime road traffic scenarios, intersections have the highest comprehensive weight. The primary reason is that intersections have a large number of vehicle-vehicle and vehicle-pedestrian conflict points, and require drivers to complete right-of-way judgment, trajectory prediction, and speed control within a very short time. This in certain will result in high cognitive load [38,39]. The comprehensive weight of access points is second only to intersections. The root of the risk lies in the trade-off between speed difference and gap acceptance behavior. Drivers waiting to merge into the main road at access points are prone to making risky merging decisions under psychological pressure and speed differences. Aggressive drivers may accept a short headway, which potentially leads to rear-end or side collisions [10,11].

The relatively high weight of bridges is related to urban infrastructure. Liuzhou City has numerous bridges, including river-crossing bridges, elevated bridges, and ordinary bridges. Particularly in nighttime rainy conditions, bridge decks are more likely to induce vehicle skidding, and drivers face difficulties in anticipating alignment changes such as curves and slopes [7]. Moreover, the areas under bridges create visual blind spots due to pier obstruction and glare interference from opposing headlights. Coupled with slippery road surfaces and dim lighting, braking distances are extended [6].

The comprehensive weight factors of each road type in the table serve as the base weights, which are superimposed with the factors obtained from the dynamic weight adjustment method. By virtue of this, the traffic risk values are calculated.

3.2. Traffic Risks Under Different Illumination and Weather

Here, we take 00:00 AM at night as an example, the traffic risks under different illumination and weather conditions were calculated according to Equation (7), as shown in Figure 4.

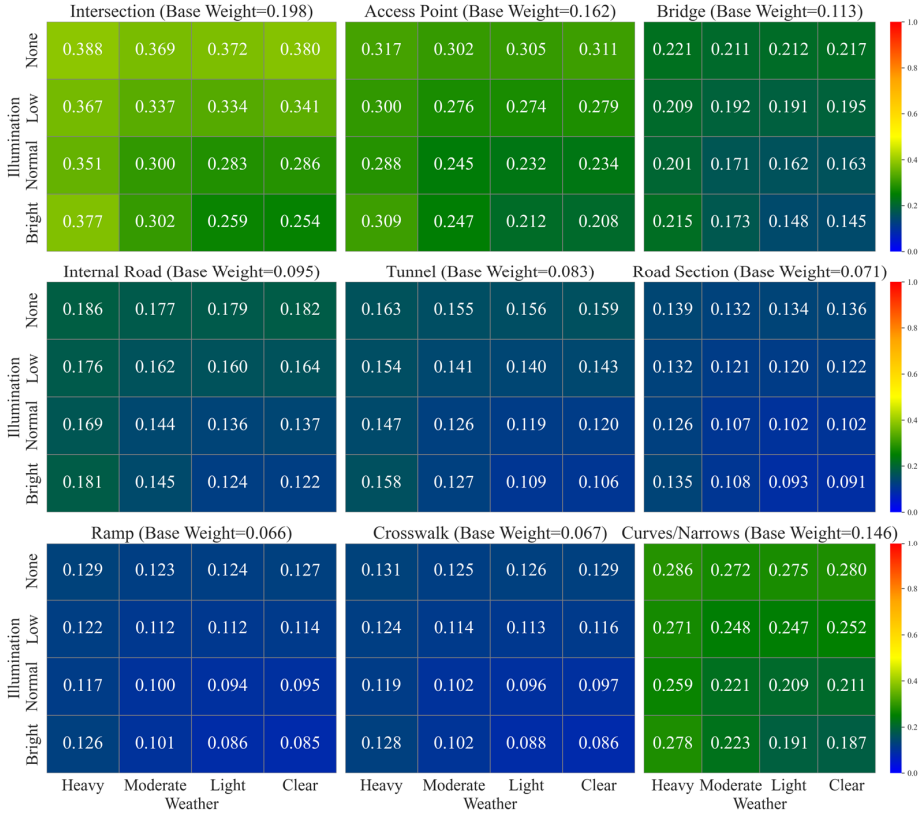


Figure 4. Risk distribution chart under various weather and illumination scenarios at 00:00.

Figure 4 illustrates the variation patterns of traffic risk with changing environmental conditions. From a horizontal comparison, intersections exhibit the highest risk values across all combinations of illumination and weather. It reaches a peak under the extreme condition of no illumination + heavy rain, which is determined by their inherent high-risk characteristics of numerous conflict points and complex decision-making [40]. Access points show a significant risk increase under clear and light rain conditions, while curves/narrow roads exhibit a substantial increase in risk with rising rainfall under bright illumination. The reason is that increased rainfall reduces the road surface adhesion coefficient, significantly lowering the critical speed for skidding. On the other hand, narrow roads often have narrow shoulders or no shoulders at all. Once skidding occurs, vehicles directly tilt toward the road edge or collide with oncoming vehicles. The risks of internal roads, tunnels, road sections, ramps, and crosswalks decrease sequentially. Crosswalks have the lowest risk under favorable lighting and clear weather conditions yet still rise significantly under adverse conditions [41].

From the perspective of illumination condition variation, all road types exhibit a consistent trend: the better the illumination, the lower the risk. Under bright illumination, the risk of each road type remains at a low level, whereas under no illumination, the risk increases sharply, especially for intersections and access points. It is noteworthy that the modeled risk of tunnels under bright illumination remains slightly higher than that of several lower-baseline road types under the same environmental conditions. This residual risk may be partly attributed to visual adaptation demands at tunnel portals, where abrupt luminance transitions between the tunnel interior and exterior can induce transient visual discomfort and the so-called black-hole/white-hole effects. Field and experimental studies have shown that such transitions produce marked changes in drivers' pupil responses and visual search behavior, and that nighttime drivers, particularly novices, may require a longer adaptation zone before and after tunnel entry [8,9]. Therefore, bright internal lighting can reduce risk but cannot completely eliminate the perceptual burden associated with portal luminance transitions [23].

From the perspective of weather conditions, heavy rain has the most significant amplifying effect on risk, followed by moderate rain, while light rain has a relatively minor impact. The risks of intersections, access points, bridges, and other road types are more sensitive to rainfall, reflecting that these road sections are more susceptible to the effects of slippery road surfaces and reduced visibility.

3.3. Traffic Risks at Different Nighttime Hours

Figure 5 shows the traffic risks varying with nighttime hours.

Figure 5 illustrates the interaction mechanism between environmental variables and time effects in nighttime traffic risk. Under the three adverse or moderate environmental combinations of no illumination + heavy rain, low illumination + moderate rain, and normal illumination + light rain, the traffic risks of all nine road types exhibit time-insensitive characteristics with slight fluctuation amplitudes. This indicates that when illumination and weather conditions constitute strong environmental stress, the regulatory effect of time factors on risk is suppressed. Also, drivers' circadian rhythms cannot manifest as gradual changes in risk under adverse environments. Instead, the increased cognitive load on drivers and vehicle handling risks causes the risk to remain at a persistently high value.

When illumination and weather conditions improve to bright and clear, traffic risk exhibits a significant decreasing trend as nighttime progresses. This variation pattern aligns well with drivers' circadian rhythms [42]. When dynamic environmental risks alleviate, endogenous factors such as driver fatigue and alertness levels which vary over time become dominant. Furthermore, the higher traffic risk during the early night (20:00–00:00)

compared to the late night (01:00–05:00) is primarily attributable to greater traffic volume. Meanwhile, favorable illumination and weather conditions tend to induce speeding behavior among drivers, resulting in greater potential traffic risk.

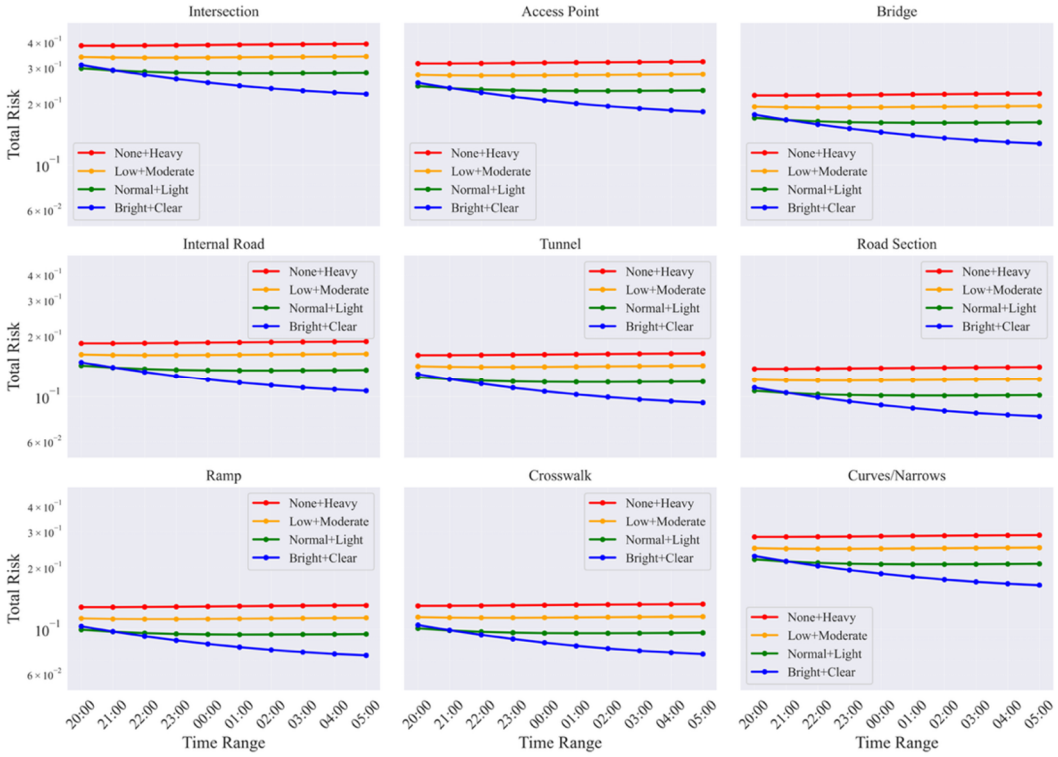


Figure 5. Risk variation graphs over nighttime hours for different road types.

It is worth noting that high-risk road types such as intersections and access points still maintain a relatively high risk baseline, but their downward slope over time is generally consistent with that of other road types. This indicates that environmental improvement and nighttime driving duration can reduce traffic risk to a certain extent, but cannot eliminate the inherent risk differences associated with road types themselves.

4. Discussion

4.1. Spatiotemporal Distribution Characteristics of Crashes

To validate the effectiveness of the established risk prediction model, this study picked out a total of 40,852 nighttime road traffic crashes (20:00 PM–6:00 AM) based on historical traffic crash data in Liuzhou City from 2018 to 2024. Figure 6 presents the traffic crash data statistics at different road types during the nighttime period from 20:00 to 06:00 in Liuzhou City from 2018 to 2024.

As shown in Figure 6, nighttime road traffic crashes are mainly distributed in locations such as straight road sections, intersections, access points, bridges, and internal roads, with the number of crashes continuously decreasing as nighttime progresses. In terms of absolute crash counts, the observed order is: road segments > intersections > entrances/exits > bridges > internal roads > tunnels > ramps > crosswalks > curves/narrow roads.

It should be noted that the crash frequencies presented in Figure 5 are absolute crash counts, which are reported to describe the observed distribution of crashes across road types. These absolute counts are influenced by the varying lengths and traffic volumes of different road types and should not be directly interpreted as exposure-adjusted risk. The AHP baseline weights, in contrast, were derived from experts' volume-adjusted fre-

quency assessments and therefore reflect a more accurate measure of inherent risk per unit of exposure.

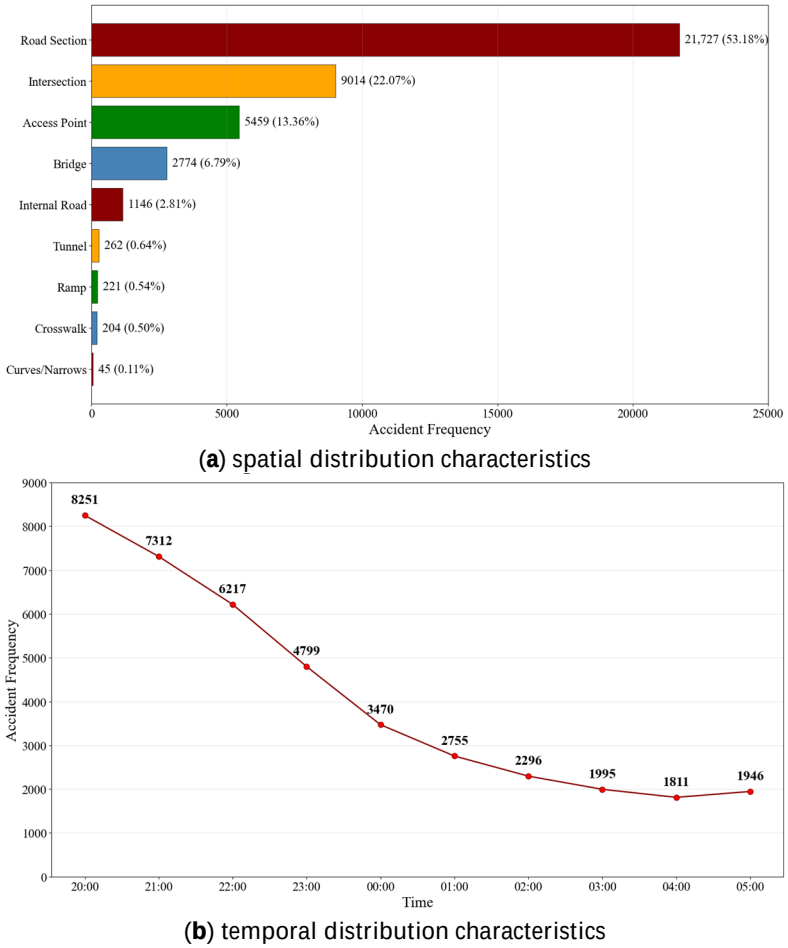


Figure 6. Spatiotemporal distribution characteristics of nighttime road traffic crashes.

The high incidence of nighttime crashes on straight road segments is mainly attributed to the high average vehicle speeds resulting from significant reduction in traffic volume compared to daytime. In addition, factors of drivers' physiological states such as fatigue, distraction, and drunk driving act as another key causations for crashes. Intersections experience elevated crash risk due to numerous vehicle-pedestrian conflict points, increased cognitive load on drivers and low traffic volume that may induce speeding or red-light running behaviors. At entrances/exits of buildings, industrial parks and residential areas, drivers have to monitor surrounding vehicles and pedestrian movements while engaging in game-theoretic driving decisions. This will uncertainly make mistakes in decisions and maneuvers. Bridges are susceptible to crashes due to high vehicle speeds on expressways or limited visibility beneath bridges. Tunnel crashes are primarily caused by the mild hypnotic effect of tunnel lighting, which may lead drivers to become less vigilant or observant, resulting in rear-end collisions. At ramps, merging drivers under psychological pressure and speed differences are likely to make erroneous judgments. Also, the visual blind spots affect drivers at the merging areas. For crosswalks and curved/narrows, crashes are mainly caused by driver distraction, sudden appearance of pedestrians or non-motorized vehicles, blind spots due to environmental obstructions, or difficulty in target recognition, though the number of such crashes is relatively low [43].

In terms of temporal distribution, road traffic volume decreases rapidly after 20:00 at night, reaching its minimum between 00:00 and 03:00.

4.2. Dynamic Risk Factors Sensitivity Analysis

Based on the crash data, sensitivity analysis was implemented to investigate the influence of risk factor further. The crash severity, crash time hour, weather, visibility, illumination were encoded as ordinal variables as shown in Table 6.

Table 6. Statistical features and the corresponding ordinal values of the nighttime crash data.

Statistic Feature	Semantic Values	Values	Variable Type
Crash Type	[property-damage-only, injury, fatal]	[1, 2, 3]	Ordinal
Illumination	[none/dark, low, normal, bright]	[1, 2, 3, 4]	Ordinal
Weather	[sunny/clear, cloudy/light rain, moderate rain/fog, heavy rain]	[1, 2, 3, 4]	Ordinal
Visibility	[>200 m, 100–200 m, 50–100 m, <50 m]	[1, 2, 3, 4]	Ordinal
Time	[20:00–05:00]	[0, 1, . . ., 9]	Ordinal

In Table 6, all the variables were treated as ordinal variables and were entered as continuous linear terms in the model. Before interpreting the regression results, the proportional odds assumption of the ordinal logit model was tested using the Brant test. The test yielded a chi-square statistic of 12.47 (df = 8, p = 0.132), indicating that the proportional odds assumption was not violated at the 5% significance level. This confirms that the effects of the explanatory variables are consistent across the cumulative logit thresholds. The results are shown in Figure 7.

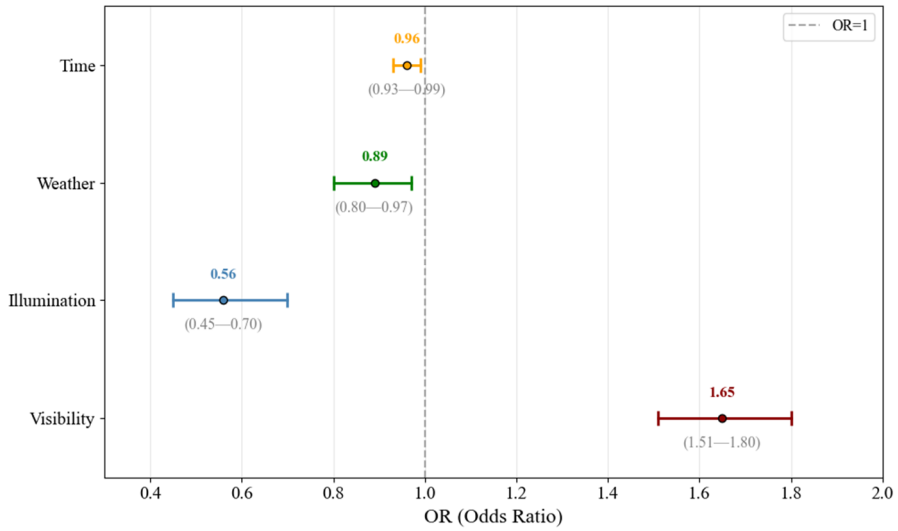


Figure 7. Contribution of traffic risk factors to crash severity.

As shown in Figure 7, the influence of various factors on the severity of nighttime traffic crashes exhibits significant differences. The odds ratio (*OR*) for visibility is 1.65 (95% *CI*: 1.51–1.80), indicating that for each one-level decrease in visibility, crash severity increases by 65%. Moreover, it is the most significant risk factor among others [44]. The *OR* for illumination conditions is 0.56 (95% *CI*: 0.45–0.70), which suggests that good lighting can reduce crash severity by 44%. Hence, enhanced lighting at night serves as a strong protective effect on reducing crash severity in nighttime environments.

The OR for weather is 0.89 (95% CI: 0.80–0.97). Since weather was coded as higher values indicating worse conditions, $OR < 1$ suggests that more severe weather is associated with lower odds of higher-severity crashes. One possible interpretation is behavioral adaptation, as drivers may reduce speed and exercise greater caution under adverse weather conditions [45,46], which could partially offset increased environmental hazards. However, the underlying mechanism cannot be confirmed with the current data, and this counterintuitive finding warrants further investigation using disaggregated data that explicitly incorporates traffic volume and real-time driving behavior. The *OR* for time is 0.96 (95% *CI*: 0.93–0.99), indicating that the odds of higher severity slightly decrease as nighttime progresses.

Furthermore, to assess the sensitivity of the model to the choice of α, we calculated the total risk scores for three representative road types (intersections, bridges, and road segments) under two environmental scenarios (no illumination with heavy rain, and bright illumination with clear weather) across a range of α values (0.5 to 2.5).

As shown in Table 7, the absolute risk scores increase with α across all scenarios. However, the relative risk ranking of road types remains stable regardless of α. The Spearman correlation between predicted risk scores and observed crash rates remains above 0.80 for α between 0.8 and 2.2, confirming the robustness of the model. The selected value $\alpha = 1.5$ offers a reasonable balance between capturing nonlinear risk amplification and avoiding excessive weight distortion.

Table 7. Sensitivity of risk scores to α for representative road types.

α	Intersection		Bridge		Segment	
	Adverse	**Favorable**	**Adverse**	**Favorable**	**Adverse**	**Favorable**
0.5	0.284	0.197	0.162	0.112	0.102	0.071
1.0	0.335	0.225	0.195	0.128	0.123	0.081
1.5	0.388	0.254	0.235	0.145	0.147	0.092
2.0	0.447	0.286	0.281	0.163	0.175	0.104
2.5	0.512	0.319	0.334	0.182	0.208	0.116

Note: Adverse denotes the condition of no illumination with heavy rain, and Favorable means bright illumination with clear weather.

Furthermore, to examine whether the AHP rankings are sensitive to the expert weighting scheme, we recomputed the comprehensive weights for all nine road types using equal weights (1:1:1) for the three expert groups and compared the results with those obtained under the original differential weighting scheme (1:2:3).

As shown in Table 8, the two schemes yield broadly consistent results. The Spearman rank correlation coefficient between the two sets of comprehensive weights is 0.983 ($p < 0.01$). The rank order of the top three road types (intersections > access points > curves/narrow roads) remains identical, and the maximum absolute difference in weight values is 0.011. This indicates that the AHP-based risk rankings are reasonably robust to the choice of expert weighting scheme, and that the differential weighting adopted in this study does not materially alter the relative risk hierarchy among road types.

Table 8. Comparison of comprehensive weights under differential and equal expert weighting.

Road Type	Differential Weight	Equal Weight	Difference
Intersection	0.198	0.187	+0.011
Access Point	0.162	0.153	+0.009
Curves/Narrow	0.146	0.151	−0.005

Table 8. *Cont.*

Road Type	Differential Weight	Equal Weight	Difference
Bridge	0.113	0.119	−0.006
Internal Road	0.095	0.099	−0.004
Tunnel	0.083	0.086	−0.003
Road Segment	0.071	0.074	−0.003
Crosswalk	0.067	0.064	+0.003
Ramp	0.066	0.067	−0.001

Note: Spearman rank correlation = 0.983 ($p < 0.01$).

4.3. Direct Validation of Risk Scores

To directly validate the total risk values calculated by our dual-layer model, we compared the model-predicted risk scores with observed crash data. For each road type, we aggregated the 40,852 nighttime crash records and calculated the observed crash rate (number of crashes per 10,000 vehicles) for each combination of environmental conditions (illumination and weather). The calculated risk scores for the corresponding scenarios were then extracted using Equation (7).

A Spearman rank correlation analysis was performed to examine the monotonic relationship between the predicted risk scores and observed crash rates across all road types and environmental scenarios. The Spearman correlation coefficient was 0.852 ($p < 0.01$), indicating a strong and statistically significant positive correlation between the model-predicted risk scores and observed crash rates. This confirms that the proposed dual-layer model effectively captures the relative risk hierarchy across different road types under varying environmental conditions.

Additionally, we calculated the Mean Absolute Percentage Error (MAPE) between the normalized risk scores and normalized crash frequencies for the nine road types under baseline conditions (normal illumination and clear weather). The MAPE was 12.3%, suggesting that the model predictions are reasonably close to the observed crash patterns.

Table 9 presents the comparison between predicted risk scores and observed crash rates for the nine road types under baseline conditions. The ranking consistency further supports the validity of the baseline weight allocation.

Table 9. Comparison of predicted risk scores and observed crash rates under baseline conditions.

Road Type	Predicted Risk Score	Observed Crash Rate (per 10,000 Vehicles)	Rank (Predicted)	Rank (Observed)
Intersection	0.198	12.4	1	1
Access Point	0.162	10.1	2	2
Curves/Narrow	0.146	8.7	3	3
Bridge	0.113	7.2	4	4
Internal Road	0.095	6.8	5	5
Tunnel	0.083	5.1	6	6
Road Segment	0.071	4.7	7	7
Crosswalk	0.067	4.2	8	9
Ramp	0.066	4.5	9	8

Note: Exposure data are derived from average annual daily traffic estimates provided by the Liuzhou traffic management bureau.

In Table 9, the predicted risk scores show a strong agreement with the observed exposure-normalized crash rates for most road types, particularly for intersections and access points, which rank among the highest in both measures. It should be noted that road segments exhibit the highest absolute crash count in Figure 6 but a moderate exposure-normalized crash rate, because they carry the largest traffic volume and account for the

largest share of the road network in terms of both number and length. This contrast confirms that absolute crash counts and exposure-normalized crash rates capture different aspects of risk, and it reinforces the rationale for using volume-adjusted frequency assessments in the AHP weighting process rather than raw crash counts.

It should also be noted that ramps and crosswalks exhibit a minor rank inversion between predicted and observed rankings. Ramps have a slightly higher observed crash rate than crosswalks, yet receive a lower predicted risk score. This discrepancy is likely attributed to the AHP baseline weights for crosswalks and ramps, which reflects experts' judgment that pedestrian-vehicle conflicts at crosswalks are more avoidable through engineering measures than the speed-differential merging conflicts at ramps. Given that the difference in both predicted scores (0.001) and observed rates (0.3 per 10,000 vehicles) is marginal, this minor inversion does not materially affect the overall validation results. Thus, the overall rank consistency between predicted risk scores and observed crash rates supports the validity of the baseline weight allocation.

4.4. Temporal Validation

To assess whether the proposed model generalizes unseen data, we conducted a temporal validation using an independent holdout design. The 40,852 nighttime crash records were divided into a calibration set (2018–2022, n = 27,086) and a validation set (2023–2024, n = 13,766). It should be clarified that the AHP baseline weights were derived from expert judgment alone, without any exposure to the crash dataset, and are therefore independent of both the calibration and validation periods. These weights were therefore held fixed at their expert-derived values throughout the temporal validation. The dynamic factor weights and the variable-weight coefficient α were re-calibrated using only the calibration set (2018–2022). Accordingly, the 2023–2024 validation records were not involved in any stage of model development, and the temporal validation is fully independent.

The parameters that were re-calibrated using only the calibration set were the data-driven parameters of the dynamic adjustment component. The baseline weights of the three dynamic factors, which were re-calibrated within $\pm$15% of the expert-proposed initial values. The calibration-set estimates were 0.46, 0.28, and 0.26, respectively. On the other hand, the variable-weight coefficient α, which was re-selected by maximizing the Spearman correlation between predicted risk scores and observed crash rates in the calibration set. The calibration-set estimate was α = 1.4.

The calibrated model was then applied to the validation set (2023–2024) without further parameter adjustment. The Spearman rank correlation coefficient between the predicted risk scores and observed crash rates in the validation set was 0.83 ($p < 0.01$), and the MAPE was 14.6%. These results are slightly lower than those from the full-sample analysis (ρ = 0.852, MAPE = 12.3%), which is expected for independent validation, but they remain strong and statistically significant. This confirms that the model generalizes well to unseen data and that its predictive capability is not an artifact of overfitting.

5. Conclusions

This work develops a dual-layer quantitative model coupled static baseline risk with dynamic environmental correction for nighttime urban road traffic risk, and conducts visualization analysis and empirical validation based on 40,852 nighttime traffic crash records from 2018 to 2024.

At the theoretical modeling level, AHP is first employed to establish a four-dimensional evaluation framework covering crash frequency, crash severity, risk controllability, and environmental sensitivity. Through group expert decision-making, comprehensive weights are determined for nine road types, and the weight allocation hierarchy

is established. The weight ranks are intersections > access points > curves/narrows > bridges > internal roads > tunnels > road segments > ramps > crosswalks. Building upon this foundation, three dynamic environmental factors which are illumination, weather, visibility and time are introduced, and the variable weight synthesis method is adopted to achieve dynamic weight adjustment.

Finally, a quantitative model for nighttime urban road traffic risk is constructed that integrates baseline risk with dynamic risk adjustment factors. The findings reveal that road type determines the risk baseline, while illumination and weather dictate the magnitude of risk fluctuation. The temporal factor demonstrates significant regulatory influence only when environmental conditions improve, with its effect being substantially suppressed under adverse conditions.

At the empirical validation level, ordinal logit regression is employed to analyze the impact of various statistical features on crash severity based on crash data. The spatial distribution analysis shows that road segments have the largest number of recorded nighttime crashes, whereas intersections exhibit the highest AHP-based baseline risk. This difference should not be interpreted as a contradiction, because the former represents absolute observed crash counts, whereas the latter represents the relative intrinsic risk characteristics of different road types. However, disaggregated exposure data at the individual crash-record level, such as vehicle-kilometers traveled and road length for each specific location, were not available.

The findings of this study carry several direct policy implications for nighttime traffic safety management. First, given that illumination provides the strongest protective effect ($OR = 0.56$) and visibility is the most significant risk factor ($OR = 1.65$), traffic authorities should prioritize upgrading lighting facilities at high-risk locations, particularly intersections, access points, and curves/narrow roads, while also installing reflective markers and active warning signs to improve visibility under low-light conditions. Second, differentiated interventions should target road types with the highest inherent risks, including optimized signal timing and dedicated turning phases at intersections, improved merge lane design at access points, and curve warning systems on narrow roads. Third, the nonlinear risk amplification under compound adverse conditions underscores the need for dynamic environmental warning systems that integrate real-time weather and lighting data to issue risk alerts and adjust speed limits accordingly. Fourth, enhanced enforcement measures, such as increased police patrols and random breath testing, are recommended during early nighttime hours (20:00–00:00) when traffic volume and risk levels are highest. Finally, in areas prone to frequent rainfall, engineering standards should mandate backup lighting and high-friction pavement treatments for high-risk road types. Collectively, these evidence-based strategies translate our quantitative risk estimates into actionable interventions that directly address the identified risk factors and contribute to safer nighttime driving environments.

However, several limitations of this study should be acknowledged. First, the analysis is based on crash data from a single city, which may limit the generalizability of the findings to other regions with different road geometries, traffic compositions, or climate conditions. Second, the thresholds for the five risk levels were determined through expert consultation rather than derived from objective psychophysical or behavioral experiments. Third, this study did not incorporate real-time driver behavior data, which could provide more nuanced insights into individual risk perception and responses. Future research should extend the model to multiple cities, calibrate risk thresholds using naturalistic driving data or driving simulator experiments, and integrate driver behavior characteristics to enrich the risk assessment framework.

Author Contributions: P.X. contributed to conceptualization, methodology, writing—original draft, writing—review & editing, and funding acquisition. G.F. was responsible for traffic crash data curation, crash investigation, and model validation. L.X. contributed to supervision, project administration, and manuscript revision. Y.P. and C.F. contributed to AHP modeling, statistical data analysis, and visualization. X.W. and J.H. contributed to crash causation analysis, model analysis, and validation. Not all CRediT roles apply to this manuscript, and some authors contributed through multiple roles. All authors have read and agreed to the published version of the manuscript.

Funding: This work presented in the paper is supported by the National Natural Science Foundation of China (Grant No. 52562054) and Guangxi Postgraduate Education Innovation Program Project (Grant No. YCSW2025571).

Data Availability Statement: The data presented in this study are available on request from the corresponding author. The data are not publicly available due to privacy and confidentiality restrictions imposed by the Traffic Police Detachment of Liuzhou Public Security Bureau.

Conflicts of Interest: Author Xingchang Wang was employed by the company Beijing Chenrong Testing Technology Co., Ltd. The remaining authors declare that the research was conducted in the absence of any commercial or financial relationships that could be construed as a potential conflict of interest. The authors declare no conflicts of interest.

References

1. Bella, F.; Calvi, A.; D'Amico, F. Analysis of driver speeds under night driving conditions using a driving simulator. *J. Saf. Res.* **2014**, *49*, 45–52. [CrossRef]
2. Peng, Z.P.; Wang, Y.G.; Wang, L.J. A comparative analysis of factors influencing the injury severity of daytime and nighttime crashes on a mountainous expressway in China. *Int. J. Inj. Control Saf. Promot.* **2021**, *28*, 503–512. [CrossRef]
3. Feng, P.F.; Liu, J.; Zhou, B. Review of driver behavior characteristics and hazard perception enhancement in low-illumination environments. *J. Adv. Transp.* **2025**, 2554540. [CrossRef]
4. Samy, S.; Gedam, V.; Karthick, S.; Sudarsan, J.S.; Anupama, C.G.; Ghosal, S.; Samuel, A.A. The drowsy driver detection for crash mitigation using facial recognition system. *Life Cycle Reliab. Saf. Eng.* **2025**, *14*, 299–311. [CrossRef]
5. Hossain, A.; Sun, X.D.; Shahrier, M.; Islam, S.; Alam, S. Exploring nighttime pedestrian crash patterns at intersection and segments: Findings from the machine learning algorithm. *J. Saf. Res.* **2023**, *87*, 382–394. [CrossRef]
6. Zhao, X.H.; Yang, H.Y.; Yao, Y.; Qi, H.; Guo, M.; Su, Y.L. Factors affecting traffic risks on bridge sections of freeways based on partial dependence plots. *Physica A Stat. Mech. Its Appl.* **2022**, *598*, 127343. [CrossRef]
7. Li, J.L.; Yan, L.; He, X.H.; Lu, T.Q. Driving safety assessment of high-sided vehicles on long-span truss suspension bridges subjected to crosswind. *J. Wind Eng. Ind. Aerodyn.* **2026**, *268*, 106287. [CrossRef]
8. Du, Z.G.; Zheng, Z.J.; Zheng, M.; Ran, B.; Zhao, X. Drivers' visual comfort at highway tunnel portals: A quantitative analysis based on visual oscillation. *Transp. Res. Part D. Transp. Environ.* **2014**, *31*, 37–47. [CrossRef]
9. Wang, Y.G.; Wang, L.J.; Wang, C.; Zhao, Y.D. How eye movement and driving performance vary before, during, and after entering a long expressway tunnel: Considering the differences of novice and experienced drivers under daytime and nighttime conditions. *SpringerPlus* **2016**, *5*, 538. [CrossRef]
10. Xu, Y.R.; Ye, Z.R.; Wang, Y.; Wang, C.; Sun, C.C. Evaluating the influence of road lighting on traffic safety at accesses using an artificial neural network. *Traffic Inj. Prev.* **2018**, *19*, 601–606. [CrossRef]
11. Mu, C.; Du, L.L.; Zhao, X.M. Event triggered rolling horizon based systematical trajectory planning for merging platoons at mainline-ramp intersection. *Transp. Res. Part C Emerg. Technol.* **2021**, *185*, 105571. [CrossRef]
12. Wang, T.; Tang, W.Z.; Chen, J.C.; Chen, W.W. Correlation analysis of influencing factors of autonomous vehicle crashs based on improved apriori algorithm. *J. Adv. Transp.* **2026**, 7024232. [CrossRef]
13. Ackaah, W.; Apuseyine, B.A.; Afukaar, F.K. Road traffic crashes at night-time: Characteristics and risk factors. *Int. J. Inj. Control Saf. Promot.* **2020**, *27*, 392–399. [CrossRef]
14. Usman, S.M.; Khattak, A.J.; Patwary, A.L. Nighttime pedestrian safety in different communities: Application of artificial intelligence techniques. *J. Saf. Res.* **2025**, *94*, 340–361. [CrossRef]
15. Plainis, S.; Murray, I.J.; Pallikaris, I.G. Road traffic casualties: Understanding the night-time death toll. *Inj. Prev.* **2006**, *12*, 125–128. [CrossRef]
16. Babić, D.; Babić, D.; Cajner, H.; Sruk, A.; Fiolić, M. Effect of road markings and traffic signs presence on young driver stress level, eye movement and behaviour in night-time conditions: A driving simulator study. *Safety* **2020**, *6*, 24. [CrossRef]

17. Myhrmann, M.S.; Mabit, S.E. Assessing bicycle crash risks controlling for detailed exposure: A Copenhagen case study. *Crash Anal. Prev.* **2023**, *192*, 107226. [CrossRef]
18. Mikoski, P.; Zlupko, G.; Owens, D.A. Drivers' assessments of the risks of distraction, poor visibility at night, and safety-related behaviors of themselves and other drivers. *Transp. Res. Part F Traffic Psychol. Behav.* **2019**, *62*, 416–434. [CrossRef]
19. Wang, K.; Zhang, W.H.; Liu, J.; Feng, Z.X.; Wang, C.L.; Hu, Z.; Huang, W.J. Exploring the factors affecting myopic drivers' driving skills and risk perception in nighttime driving. *Cogn. Work* **2019**, *21*, 275–285. [CrossRef]
20. Evans, T.; Stuckey, R.; Macdonald, W. Young drivers' perception of hazards: Variation with experience and day versus night. *Transp. Res. Part F Traffic Psychol. Behav.* **2022**, *88*, 258–280. [CrossRef]
21. Tamakloe, R.; Khorasani, M.; Kim, I. Differences in injury severities between elderly and non-elderly taxi driver at-fault crashes: Temporal instability and out-of-sample prediction. *Crash Anal. Prev.* **2025**, *211*, 107865. [CrossRef]
22. Zhang, K.R.; Hassan, M. Crash severity analysis of nighttime and daytime highway work zone crashes. *PLoS ONE* **2019**, *14*, e0221128. [CrossRef]
23. Yang, D.; Zuo, F.; Ozbay, K.; Gao, J.Q. Drivers' reactions to real-world forward collision warnings at both macroscopic and microscopic longitudinal levels: A functional approach. *Crash Anal. Prev.* **2025**, *210*, 107853. [CrossRef]
24. Kaduk, S.I.; Roberts, A.P.J.; Stanton, N.A. The manual shift in phase: The impact of circadian phase on semi-autonomous driving. What can we learn from current understanding in manual driving? *Theor. Issues Ergon. Sci.* **2021**, *22*, 103–123. [CrossRef]
25. Le, K.G.; Tran, Q.H.; Do, V.M. Urban traffic crash features investigation to improve urban transportation infrastructure sustainability by integrating GIS and data mining techniques. *Sustainability* **2024**, *16*, 107. [CrossRef]
26. Xu, C.; Zhang, Z.M.; Fu, F.J.; Yao, W.B.; Su, H.Y.; Hu, Y.W.; Rong, D.L.; Jin, S. Analysis of Spatiotemporal Factors Affecting Traffic Safety Based on Multisource Data Fusion. *J. Transp. Eng. Part A Syst.* **2023**, *149*, 04023098. [CrossRef]
27. Qu, Q.K.; Shen, Y.J.; Yang, M.M.; Zhang, R. Towards efficient traffic crash detection based on macro and micro data fusion on expressways: A digital twin framework. *IET Intell. Transp. Syst.* **2024**, *18*, 2725–2743. [CrossRef]
28. Yumak, A.; Tercan, S.H.; Colak, U.C.; Ozcanan, S. A machine learning approach to identify high-risk road segments and crash severity patterns based on categorical data. *Appl. Sci.* **2025**, *15*, 12824. [CrossRef]
29. Goniewicz, K.; Goniewicz, M.; Pawłowski, W.; Fiedor, P. Road crash rates: Strategies and programmes for improving road traffic safety. *Eur. J. Trauma Emerg. Surg.* **2016**, *42*, 433–438. [CrossRef]
30. Aldoski, Z.N.; Koren, C. Traffic sign detection and quality assessment using YOLOv8 in daytime and nighttime conditions. *Sensors* **2025**, *25*, 1027. [CrossRef]
31. Chien, J.C.; Chen, Y.S.; Lee, J.D. Mproving night time driving safety using vision-based classification techniques. *Sensors* **2017**, *17*, 2199. [CrossRef]
32. Shen, J.H.; Li, G.F.; Yan, W.Q.; Tao, W.J.; Xu, G.; Diao, D.F.; Green, P. Nighttime driving safety improvement via image enhancement for driver face detection. *IEEE Access* **2018**, *6*, 45625–45634. [CrossRef]
33. Zhang, G.N.; Yau, K.W.; Gong, X.P. Traffic violations in Guangdong Province of China: Speeding and drunk driving. *Crash Anal. Prev.* **2014**, *64*, 30–40. [CrossRef]
34. Park, S.; Akar, G. Linking built environments and pre-crash pedestrian behaviors: A Safe Systems approach to crash severity. *Traffic Inj. Prev.* **2026**, 1–10. [CrossRef]
35. *CJJ 45-2015*; Standard for Lighting Design of Urban Roads. Ministry of Housing and Urban-Rural Development of the People's Republic of China: Beijing, China, 2015.
36. Murdoch, W.J.; Singh, C.; Kumbier, K.; Abbasi-Asl, R.; Yu, B. Interpretable machine learning: Definitions, methods, and applications. *Proc. Natl. Acad. Sci. USA* **2019**, *116*, 22071–22080. [CrossRef]
37. Mannering, F.L.; Shankar, V.; Bhat, C.R. Unobserved heterogeneity and the statistical analysis of highway crash data. *Anal. Methods Crash Res.* **2016**, *11*, 1–16. [CrossRef]
38. Khademi, N.; Mazloum, S.; Zabihpour, A.; Chen, A. Designing safer intersections: Exploring the impact of visual and auditory warnings on pedestrian behavior in a virtual simulated environment. *Saf. Sci.* **2024**, *178*, 106604. [CrossRef]
39. Zhong, L.X.; Geng, M.S.; Wu, F.; Chen, X.Q. Intention transformer for driving intention and trajectory prediction in dilemma zones of signalized intersection. *Transp. Res. Part C Emerg. Technol.* **2026**, *185*, 105571. [CrossRef]
40. Ali, Y.; Washington, S.; Haque, M.M. Estimating real-time crash risk at signalized intersections: A Bayesian Generalized Extreme Value approach. *Saf. Sci.* **2023**, *164*, 106181. [CrossRef]
41. Osorio-García, D.; Hernández-Pulgarín, G.; Escobar, D.A. Profiles of pedestrian risk behavior while crossing the street. *Saf. Sci.* **2023**, *163*, 106120. [CrossRef]
42. Scholz, M.; Lakaemper, S.; Keller, K.; Dobay, A.; Steuer, A.E.; Landolt, H.P.; Kraemer, T. Metabolomics-based sleepiness markers for risk prevention and traffic safety (ME-SMART): A monocentric, controlled, randomized, crossover trial. *Trials* **2023**, *24*, 131. [CrossRef]
43. Leibowitz, H.W.; Owens, D.A.; Tyrrell, R.A. The assured clear distance ahead rule: Implications for nighttime traffic safety and the law. *Crash Anal. Prev.* **1998**, *30*, 93–99. [CrossRef]

44. Sadeghi, P.; Goli, A. Investigating the impact of pavement condition and weather characteristics on road crashs. *Int. J. Crashworthiness* **2024**, *29*, 973–989. [CrossRef]
45. Edwards, J.B. The temporal distribution of road crashs in adverse weather. *Meteorol. Appl.* **1999**, *6*, 59–68. [CrossRef]
46. Bergel-Hayat, R.; Debbarh, M.; Antoniou, C.; Yannis, G. Explaining the road crash risk: Weather effects. *Crash Anal. Prev.* **2013**, *60*, 456–465. [CrossRef]

Disclaimer/Publisher's Note: The statements, opinions and data contained in all publications are solely those of the individual author(s) and contributor(s) and not of MDPI and/or the editor(s). MDPI and/or the editor(s) disclaim responsibility for any injury to people or property resulting from any ideas, methods, instructions or products referred to in the content.